In vitro assessment of BBI608 in 2D and 3D culture models for drug repositioning in oral squamous cell carcinoma

DONG-GUK PARK[1], HYUN-JI KIM[1], SAK LEE[1], HYE-MI JANG[1], SEONG-DOO HONG[1], SU-JUNG CHOI[1] and SUNG-DAE CHO[1,2]

[1]Department of Oral Pathology, School of Dentistry and Dental Research Institute, Seoul National University, Seoul 03080, Republic of Korea; [2]Center of Excellence in Genomics and Precision Dentistry, Department of Physiology, Faculty of Dentistry, Chulalongkorn University, Bangkok 10330, Thailand

Received October 17, 2024; Accepted April 30, 2025

DOI: 10.3892/or.2025.8930

Abstract. STAT3 is abnormally activated in several types of cancer, and elevated nuclear levels of STAT3 are strongly associated with poor prognosis in oral squamous cell carcinoma (OSCC). Despite ongoing progress in developing targeted therapies, there is no Food and Drug Administration-approved drug currently targeting STAT3 in OSCC. To evaluate the anticancer effects of BBI608, a potent STAT3 inhibitor, in two human OSCC cell lines (HSC-3 and HSC-4), various two-dimensional (2D) or 3D *in vitro* analyses were performed, including western blot analysis, colony formation assay, DAPI staining, sub-G_1 population analysis and Annexin V/PI staining. The molecular mechanisms of BBI608 were also determined using cross-linking assay, nuclear and cytoplasmic fractionation assay, reverse transcription-quantitative PCR and chromatin immunoprecipitation assay. In the present study, it was observed that human HSC-3 and HSC-4 OSCC cells exhibited higher levels of phosphorylated (p)-STAT3 compared with those in immortalized oral keratinocytes (iHOK cells). BBI608 inhibited cell proliferation in a concentration-dependent manner and triggered caspase 3-dependent apoptosis in HSC-3 and HSC-4 cells. Additionally, BBI608 reduced the nuclear translocation of p-STAT3 in HSC-3 and HSC-4 cells compared with that in DMSO-treated cells. Mechanistically, BBI608 modulated anti-apoptotic STAT3 downstream genes: Survivin expression was regulated at the transcriptional level, while myeloid cell leukemia-1 expression was modulated post-translation via proteasomal degradation. Consistent with the results from 2D culture, BBI608 showed effective anticancer effects against OSCC spheroids in 3D culture. These results suggest that BBI608 effectively inhibits STAT3 activation in both 2D and 3D models, offering a promising therapeutic strategy and supporting its potential for repurposing in patients with OSCC who exhibit elevated STAT3 activity.

Correspondence to: Dr Su-Jung Choi or Professor Sung-Dae Cho, Department of Oral Pathology, School of Dentistry and Dental Research Institute, Seoul National University, 101 Daehak-ro, Jongno, Seoul 03080, Republic of Korea
E-mail: anna47408@snu.ac.kr
E-mail: efiwdsc@snu.ac.kr

Key words: apoptosis, BBI608, drug repositioning, oral squamous cell carcinoma, STAT3

Introduction

Drug repositioning involves identifying new therapeutic applications for existing drugs beyond their original indications by uncovering novel effects or targets. This approach offers considerable advantages over traditional drug development, including shorter development timelines and lower costs, as the safety profile of the drug is already known (1). A well-known example is aspirin, initially developed as an analgesic, which has since been repurposed for its anti-platelet properties, reducing the risk of cardiovascular thrombosis, and preventing colon cancer (2). Likewise, the demand for drug repurposing in oncology has surged in recent decades (3).

STAT3 transcriptionally regulates a wide range of genes that drive key cancer hallmarks, including sustained proliferation and resistance to apoptosis and chemotherapy, such as survivin and myeloid cell leukemia-1 (Mcl-1) (4,5). Increased nuclear localization of phosphorylated (p)-STAT3 has been shown to play a critical role in tumor initiation and development, including breast and prostate cancer (6,7). Hyperactivation of STAT3 is frequently observed in advanced clinical stages of oral squamous cell carcinoma (OSCC) and is associated with poor overall survival (8,9). Given this evidence, STAT3 represents a promising target for cancer therapy. However, despite efforts to develop new drugs targeting STAT3 over the past decades, important advancements have been elusive due to various challenges, including inadequate drug delivery and unwanted side effects (5). Therefore, developing novel STAT3-targeted therapies with established safety and efficacy profiles remains a promising strategy for cancer treatment.

BBI608, an orphan drug approved by the Food and Drug Administration for treating patients with advanced gastric cancer, is a first-in-class cancer stemness inhibitor that targets STAT3 signaling (10,11). BBI608 has demonstrated tolerability and potential efficacy, such as cancer stemness inhibition and

chemosensitization, in patients with advanced solid tumors, as a monotherapy and in combination with conventional chemotherapies in early-phase clinical trials (12,13). In line with clinical trials results, BBI608 exhibited strong antitumor activity and markedly improved survival outcomes in various preclinical tumor models, including nude mouse tumor xenograft models and orthotopic tumor animal models (14). However, the anticancer effects and underlying mechanisms of BBI608 in human OSCC remain unexplored.

The present study, for the first time to the best of our knowledge, aimed to investigate the anticancer effects of BBI608 in both conventional two-dimensional (2D) and spheroid OSCC cultures, and to discover the regulatory mechanisms through which BBI608 influences its downstream target genes, survivin and Mcl-1, examining the potential of BBI608 as a therapeutic option for patients with OSCC exhibiting high STAT3 expression.

Materials and methods

Cell culture and pharmacological chemicals. The iHOK cell line (accession no. CVCL_C191) was gifted by Kyung Hee University (Seoul, South Korea). The HSC-2 (accession no. CVCL_1287), HSC-3 (accession no. CVCL_1288) and HSC-4 (accession no. CVCL_1289) cell lines were kindly provided by Hokkaido University (Sapporo, Japan). The HN22 cell line (accession no. CVCL_5522) was provided by Dankook University (Cheonan, South Korea). For 2D culture, OSCC cell lines were cultured in DMEM/F-12 medium (Welgene, Inc.) and the iHOK cell line was cultured in KBM™ Gold Keratinocyte Growth Basal Medium (Lonza Group, Ltd), supplemented with 10% fetal bovine serum (Welgene, Inc.) and 1% penicillin/streptomycin (Welgene, Inc.), in a humidified atmosphere at 37˚C with 5% CO_2. For 3D culture, OSCC spheroids were generated using a hanging drop assay (15). Briefly, 5,000 cells in 20 μl complete medium containing 0.24% methylcellulose (cat. no. M0387; Sigma-Aldrich; Merck KGaA) were plated on the lid of 100-mm dishes, which were then inverted over dishes containing 6 ml of PBS. After a 3-day incubation at 37˚C, spheroids were transferred to poly(2-hydroxyethyl methacrylate) (HEMA)-coated 96-well or 6-well plates for further experiments. To prepare poly-HEMA-coated plates, each well of uncoated 96-well or 6-well plates was filled in with 0.5% poly-HEMA in 95% ethanol and then incubated for 2 days at 37˚C. BBI608 was purchased from MedChemExpress (cat. no. HY-13919), dissolved in DMSO, and stored at -20˚C. Z-VAD-FMK was obtained from R&D Systems, Inc., while cycloheximide (CHX) and MG132 were sourced from Sigma-Aldrich (Merck KGaA) and Santa Cruz Biotechnology, Inc., respectively. HSC-3 and HSC-4 cells were pretreated with 10 and 5 μM Z-VAD-FMK, 50 and 100 ng/ml CHX and 300 and 500 nM MG132 for 1 h at 37˚C. DMSO was used as control and its concentration did not exceed 0.1%.

Western blot analysis. Cells (iHOK, HSC-2, HSC-3, HSC-4 and HN22) were lysed using RIPA lysis buffer (MilliporeSigma) supplemented with protease inhibitors (Roche Applied Science) and phosphatase inhibitors (Thermo Fisher Scientific, Inc.). For 3D culture, spheroids were sonicated on ice for 5 cycles (frequency, 20 kHz;5 sec of sonication and rest) with a Vibra-Cell VCX500 sonicator (Sonics & Materials, Inc.). Total protein concentrations were measured with the DC Protein Assay kit (Bio-Rad Laboratories, Inc.), followed by separation on 10-15% SDS-PAGE gels depending on protein size and transfer to PVDF membranes. A total of 30-50 μg protein was loaded per lane. After blocking with 5% skimmed milk (cat. no. 232100; Becton, Dickinson and Company) for 2 h at room temperature (RT), the membranes were incubated overnight at 4˚C with the specified primary antibodies. The membranes were then treated with HRP-conjugated goat anti-rabbit IgG (1:2,000; cat. no. GTX213110-01; GeneTex, Inc.) and goat anti-mouse IgG (1:2,000, cat. no. GTX213111-01, GeneTex, Inc.) for 2 h at RT. Immunoreactive signals were visualized using the WestGlow™ PICO PLUS ECL Chemiluminescent Substrate (BIOMAX) on X-ray film. Densitometric analyses were performed with ImageJ software version 1.54f (National Institutes of Health). The primary antibodies used were as follows: STAT3 (1:5,000; cat. no. 4904), p-STAT3^{Tyr705} (1:2,000; cat. no. 9145), p-STAT3^{Ser727} (1:2,000; cat. no. 9134), poly(ADP-ribose) polymerase (PARP; 1:2,000; cat. no. 9542), cleaved (c)-PARP (1:2,000; cat. no. 9541), caspase 3 (1:3,000; cat. no. 14220), c-caspase 3 (1:1,000; cat. no. 9664), survivin (1:1,000; cat. no. 2802), Mcl-1 (1:2,000; cat. no. 5453), Bcl-xL (1:5,000; cat. no. 2764), p-Mcl-1$^{Ser159/Thr163}$ (1:1,000; cat. no. 4579), p-ERK1/2$^{Thr202/Tyr204}$ (1:5,000; cat. no. 9101) and ERK1/2 (1:5,000; cat. no. 9102) were purchased from Cell Signaling Technology, Inc. Bcl-2 (1:1,000; cat. no. sc-7382), β-actin (1:5,000; cat. no. sc-47778), α-tubulin (1:5,000; cat. no. sc-5286), p-GSK3β^{Ser9} (1:1,000; cat. no. sc-373800) and GSK3β (1:1,000; cat. no. sc-377213) were purchased from Santa Cruz Biotechnology, Inc. Histone H3 (1:5,000; cat. no. ab1791; Abcam) was kindly provided by Kangwon National University (Chuncheon, South Korea).

Cell Counting Kit-8 (CCK-8) assay. Cell viability was assessed using the CCK-8 assay (Dojindo Laboratories, Inc.) following the manufacturer's instructions. For 2D culture, cells ($5x10^4$ cells/well) were seeded into 96-well plates overnight and then treated with the specified concentrations (0.1-10 μM) of BBI608 for 22 h at 37˚C. Subsequently, a 10-μl CCK-8 solution was added to each well and incubated at 37˚C with 5% CO_2 for 2 h. For 3D culture, spheroids ($5x10^5$ cells/well) were transferred to poly-HEMA-coated U-bottom 96-well plates (16) and treated with the indicated concentrations (2.5 μM for HSC-3 and 20 μM for HSC-4) of BBI608 for 6 h, followed by CCK-8 treatment for an additional 18 h. The mixture of CCK-8 and media was then transferred to a new 96-well plate, and absorbance at 450 nm was measured using a microplate reader (Hidex Oy).

Crystal violet staining. Crystal violet staining was used to visually assess the number of viable OSCC cells (HSC-3 and HSC-4) following BBI608 treatment. Briefly, cells ($2.5x10^5$ cells/well) were plated into 6-well plates overnight and then treated with various concentrations (0.125-10 μM) of BBI608 at 37˚C. After 24 h, the media containing BBI608 was removed, and the cells were washed twice with PBS. Next, the cells were fixed with 100% methanol for 2 min and stained with a 1% crystal violet solution diluted in 20% methanol for 30 min at RT. The stained cells were then photographed using an inverted light microscope (Nikon Corporation).

Trypan blue exclusion assay. OSCC cell lines (HSC-3 and HSC-4) seeded onto 6-well plate ($2.5x10^5$ cells/well) were treated with DMSO (0.1%) or BBI608 (0.2-3.2 μM) for 24 h at 37˚C. Trypan blue solution in a concentration of 0.4% (Corning, Inc.) was used to stain the cells for 3 min at a 1:1 v/v ratio at RT. Subsequently, cell viability was examined using a CytoSMART automatic cell counter (Corning, Inc.).

Colony formation assay. A total of 3 ml 1.25% agar solution was poured into 6-well plates and allowed to solidify at RT for 1-2 h. Cells ($2.4x10^4$ cells/well) were suspended in 10% Basal Medium Eagle (Sigma-Aldrich; Merck KGaA) and mixed with agar before 1 ml of this cell mixture was layered on top of the solidified agar in the plates. After the top layer solidified at RT for 1-2 h, the plates were incubated in a humidified incubator at 37˚C with 5% CO_2 for ~2 weeks. Specific concentrations of BBI608 (0.4 μM for HSC-3 and 3.2 μM for HSC-4) were added to both the bottom and top agar layers before agar solidified. The colonies (>3-pixel size; cells were not fixed or stained) that formed were visualized using a CKX53 microscope (Olympus Corporation). To prevent potential bias, each well was divided into four quadrants, and non-overlapping images were captured separately from each quadrant. These images were merged and quantified with ImageJ software version 1.54f.

DAPI staining. Following a 24-h treatment with specific concentrations (0.4 μM for HSC-3 and 3.2 μM for HSC-4) of BBI608 in OSCC cell lines seeded onto 6-well plates ($2.5x10^5$ cells/well) at 37˚C, adherent and detached cells were collected and fixed in 70% ethanol at -20˚C overnight. The fixed cells were then resuspended in 100% methanol at RT for 10 min. The cells were transferred onto glass slides and stained with a 2 μg/ml DAPI solution at RT for 1-5 min. Images of the stained cells were captured using a fluorescence microscope (Leica DMi8; Leica Microsystems GmbH).

Measurement of cell cycle distribution. HSC-3 and HSC-4 cells were seeded onto a 6-well plate ($2.5x10^5$ cells/well) and fixed overnight at -20˚C with 70% ethanol. After removing the supernatant, the cells were stained with a PI solution containing 20 μg/ml RNase A for 15 min at 37˚C. Cell cycle distribution was assessed using 10,000 cells/sample with an LSRFortessa X-20 flow cytometer (BD Biosciences) and the sub-G_1, G_1, S, and G_2/M populations were analyzed using FlowJo software (FlowJo LLC; BD Biosciences). The gating strategy of cell cycle distribution is presented in Fig. S1.

Annexin V-FITC/PI double staining. Apoptotic cells were examined using the FITC-Annexin V Apoptosis Detection Kit (cat. no. 556547; BD Biosciences). The cells collected from a 60 mm^2 dish (seeding concentration, $2.5x10^5$ cells/ml) were resuspended in 400 μl Annexin V binding buffer, which included 5 μl FITC-conjugated Annexin V and 1 μl PI solution, at RT in the dark. The stained cells were analyzed with the LSRFortessa X-20 flow cytometer, and the percentage of the apoptotic cell population was calculated using FlowJo software.

Cross-linking assay. The cross-linking assay was conducted as previously described (17). Briefly, cells (HSC-3 and HSC-4) were suspended in a conjugation buffer containing 10 mM EDTA (dissolved in PBS). The cell lysates were then incubated with 0.2 mM bismaleimidohexane (cat. no. 22330; Thermo Fisher Scientific, Inc.) at RT for 1 h, followed by extraction with lysis buffer for western blotting, as aforementioned.

Subcellular fractionation of the nucleus and cytoplasm. Nuclear and cytoplasmic proteins were extracted using the NE-PER™ Nuclear and Cytoplasmic Extraction Reagents kit (cat. no. 78833; Thermo Fisher Scientific, Inc.). Briefly, harvested cells (HSC-3 and HSC-4) were vortexed with Cytoplasmic Extraction Reagent I and incubated on ice for 10 min. The cells were then resuspended in Cytoplasmic Extraction Reagent II for 1 min and centrifuged at 13,000 g for 5 min at 4˚C. The supernatant, containing cytoplasmic proteins, was transferred to a pre-chilled Eppendorf tube (the cytoplasmic fraction). The pellets were resuspended in Nuclear Extraction Reagent and incubated for 40 min at 4˚C, with vortexing every 10 min and thorough sonication on ice for 5 cycles (frequency, 20 kHz; 2 sec of sonication and rest). The solution was then centrifuged at 13,000 g for 10 min at 4˚C. The supernatant containing nuclear proteins (the nuclear fraction) was used for western blot analysis.

Reverse transcription-quantitative PCR (RT-qPCR). Total RNA was extracted using TRIzol® reagent (cat. no. 15596026; Thermo Fisher Scientific, Inc.) and the quantity of RNA was measured with NanoPhotometer N50 (IMPLEN). Reverse transcription of 1 μg total RNA was performed using the AMPIGENE cDNA Synthesis Kit (Enzo Life Sciences, Inc.). The resulting cDNA was then analyzed by qPCR with the AMPIGENE qPCR Green Mix Hi-Rox (Enzo Life Sciences, Inc.) using the StepOnePlus™ Real-Time PCR System (Applied Biosystems; Thermo Fisher Scientific, Inc.). The PCR conditions for all genes were as follows: An initial step at 95˚C for 2 min, followed by 40 cycles of 95˚C for 10 sec and 60˚C for 30 sec. The relative expression of each gene was determined using the $2^{-\Delta\Delta Cq}$ method (18) and normalized to GAPDH as an internal control. All primers were synthesized by Cosmo Genetech Co., Ltd., with the following sequences: Mcl-1 (accession no. NG_029069.1) sense, 5'-GTATCACAGACGTTCTCGTAAGG-3' and anti-sense, 5'-CCACCTTCTAGGTCCTCTACA T-3'; survivin (accession no. NG_029146.2) sense, 5'-ACTTGGCCCAGT GTTTCTT-3' and antisense, 5'-GACAGAAAGGAAAGC GCAAC-3'; GAPDH (accession no. NG_007073.2) sense, 5'-GTGGTCTCCTCTGACTTCAAC-3' and antisense, 5'-CCTGTTGCTGTAGCCAAATTC-3'.

Chromatin immunoprecipitation (ChIP) assay. A ChIP kit from Abcam (cat. no. ab500) was used according to the manufacturer's instructions. Briefly, cells (HSC-3 and HSC-4) were harvested and cross-linked with 1.1% formaldehyde for 10 min at RT, and the reaction was then quenched with 1.25M glycine for an additional 10 min at RT. Chromatin was sheared using a Vibra-Cell VCX500 sonicator on ice for 20 cycles, alternating between 15 sec of sonication and rest (frequency, 20 kHz). In each of the three independent experiments, DNA fragments ranging from 200 to 500 base pairs were verified by electrophoresis on a 1.5% agarose gel. The sheared chromatin was incubated overnight at 4˚C with either a rabbit isotype IgG

antibody (0.24 μg, cat. no. 3900; Cell Signaling Technology, Inc.) or a rabbit STAT3 antibody (0.24 μg, cat. no. 4904; cell Signaling Technology, Inc.). After immunoprecipitation, cross-linking was reversed by adding DNA purification slurry and proteinase K (both contained within the ChIP kit used). The purified DNA was then amplified via RT-qPCR using primers targeting the known STAT3 binding site on the survivin promoter region (19). The primer sequences were as follows: Survivin sense, 5'-CAGTGAGCTGAGATCATG CC-3' and antisense, 5'-TATTAGCCCTCCAGCCCCAC-3'.

Live/dead assay. The presence of live and dead cells in the spheroids was assessed using the LIVE/DEAD™ Viability/Cytotoxicity Kit (cat. no. L3224; Thermo Fisher Scientific, Inc.), following the manufacturer's instructions. Briefly, spheroids ($5x10^5$ cells/well) were transferred into poly-HEMA-coated 96-well plates and treated with the specified concentration (2.5 μM for HSC-3 and 20 μM for HSC-4) of BBI608 for 24 h at 37˚C. Calcein AM (4 mM) and ethidium homodimer-1 (2 mM) (Themo Fisher Scientific, Inc.) were added to each well in PBS at final concentrations of 4 and 2 μM, respectively, and the spheroids were incubated for 1 h at RT. The spheroids were then visualized using a digital inverted fluorescence microscope (Nikon Corporation).

Statistical analysis. All graphs were generated using GraphPad Prism version 8.4.2 (GraphPad; Dotmatics), and statistical analyses were performed using SPSS version 25.0 (IBM Corp.). Data are presented as the mean ± SD from at least three independent experiments. A two-tailed unpaired Student's t-test was used for comparisons between two groups, while one-way ANOVA followed by Tukey's post hoc test was applied for multiple comparisons. $P<0.05$ was considered to indicate a statistically significant difference.

Results

BBI608 inhibits growth and induces apoptosis in OSCC cell lines. To select OSCC cell lines with high STAT3 activity for subsequent experiments, the protein levels of p-STAT3 at the tyrosine 705 residue were screened across a panel consisting of one immortalized human oral keratinocyte and four OSCC cell lines. Among them, HSC-3 and HSC-4 cells showed the highest levels of p-STAT3 (Fig. 1A). To evaluate the cytotoxic effects of BBI608 on OSCC cell lines, a CCK-8 assay and crystal violet staining were performed. The results indicated that BBI608 inhibited the growth of both OSCC cell lines and normal oral keratinocytes in a concentration-dependent manner (Fig. S2). The IC_{50} values for iHOK, HSC-3, HSC-4 and HN22 were 3.56, 0.57, 2.16 and 3.58 μM, respectively. The optimal concentrations of BBI608 (0.6 μM for HSC-3 and 3.2 μM for HSC-4) that inhibit STAT3 activation and simultaneously inhibit cell growth and induce the expression of c-PARP were examined using trypan blue exclusion assay (Fig. S3A) and western blot analysis (Fig. S3B). It was also observed that BBI608 treatment significantly reduced colony forming efficiency in HSC-3 and HSC-4 cell lines (Fig. 1B). To determine whether the cytotoxicity of BBI608 was mediated by apoptosis, which is characterized by nuclear condensation and DNA fragmentation, DAPI staining and cell cycle analysis were performed (20). The results revealed that BBI608 significantly increased the presence of condensed nuclei and the sub-G_1 population compared with those in DMSO-treated cells (Figs. 1C and D and S5A). Additionally, an increase in Annexin V-positive cells and enhanced cleavage of PARP and caspase 3 following BBI608 treatment was observed in HSC-3 and HSC-4 cells (Fig. 1E and F). To investigate whether BBI608-mediated apoptosis was dependent on caspase activation, OSCC cell lines were treated with Z-VAD-FMK, a pan-caspase inhibitor, at the concentrations used in our previous studies (21-23). Based on preliminary results, the minimum concentrations (10 μM for HSC-3 and 5 μM for HSC-4) of Z-VAD-FMK required to hinder PARP cleavage were selected (Fig. S4), and it was observed that BBI608-mediated apoptosis was significantly rescued by Z-VAD-FMK (Figs. 1G and S5B). Collectively, these findings demonstrated that BBI608 exhibited strong growth-inhibitory effects and induced apoptosis in OSCC cell lines.

BBI608 inhibits STAT3 activity and the expression of STAT3 target genes in OSCC cell lines. To determine whether BBI608 could inhibit STAT3 translocation into the nucleus in OSCC cell lines, western blot analysis after BBI608 treatment was performed. The results showed that BBI608 effectively suppressed STAT3 activation at both tyrosine 705 and serine 727 residues (Fig. 2A). Additionally, BBI608 effectively inhibited STAT3 dimerization compared with that in DMSO-treated cells (Fig. 2B), indicating that BBI608 may inhibit p-STAT3 nuclear translocation (24). Interestingly, BBI608 significantly reduced nuclear p-STAT3 levels at both tyrosine 705 and serine 727 residues (Fig. 2C). Next, it was investigated whether BBI608 could inhibit the expression of STAT3-regulated genes that are related to apoptosis (25,26). The results demonstrated that BBI608 significantly downregulated survivin and Mcl-1 expression, while Bcl-2 expression was increased only in HSC-4 cells and Bcl-xL was not changed in either cell line (Fig. 2D). Furthermore, BBI608 reduced the level of p-STAT3 and those of its downstream target genes, accompanied by an increase in c-PARP expression, in a time-dependent manner (Fig. S6). Overall, these findings indicated that BBI608 effectively inhibited STAT3 activation and induced apoptosis in OSCC cell lines, at least in part by inhibiting the STAT3 signaling pathway.

BBI608 regulates the expression of survivin at the transcriptional level. To evaluate how BBI608 regulates survivin and Mcl-1 in OSCC cell lines, their mRNA levels were measured over time after treatment with BBI608 in HSC-3 and HSC-4 cells. Interestingly, the results showed that BBI608 induced a significant decrease in survivin mRNA levels at all time points, while significantly increasing Mcl-1 mRNA levels in both cell lines (Fig. 3A). To further investigate whether the reduction in survivin expression was transcriptionally regulated by BBI608 treatment in response to decreased STAT3 activation, a ChIP assay was performed. The results revealed that BBI608 significantly impaired STAT3 binding to the survivin promoter region in HSC-3 and HSC-4 cells, which was larger than the binding impairment in the IgG control group (Fig. 3B). These findings suggested that BBI608 may regulate survivin expression through a transcriptional mechanism in OSCC cell lines.

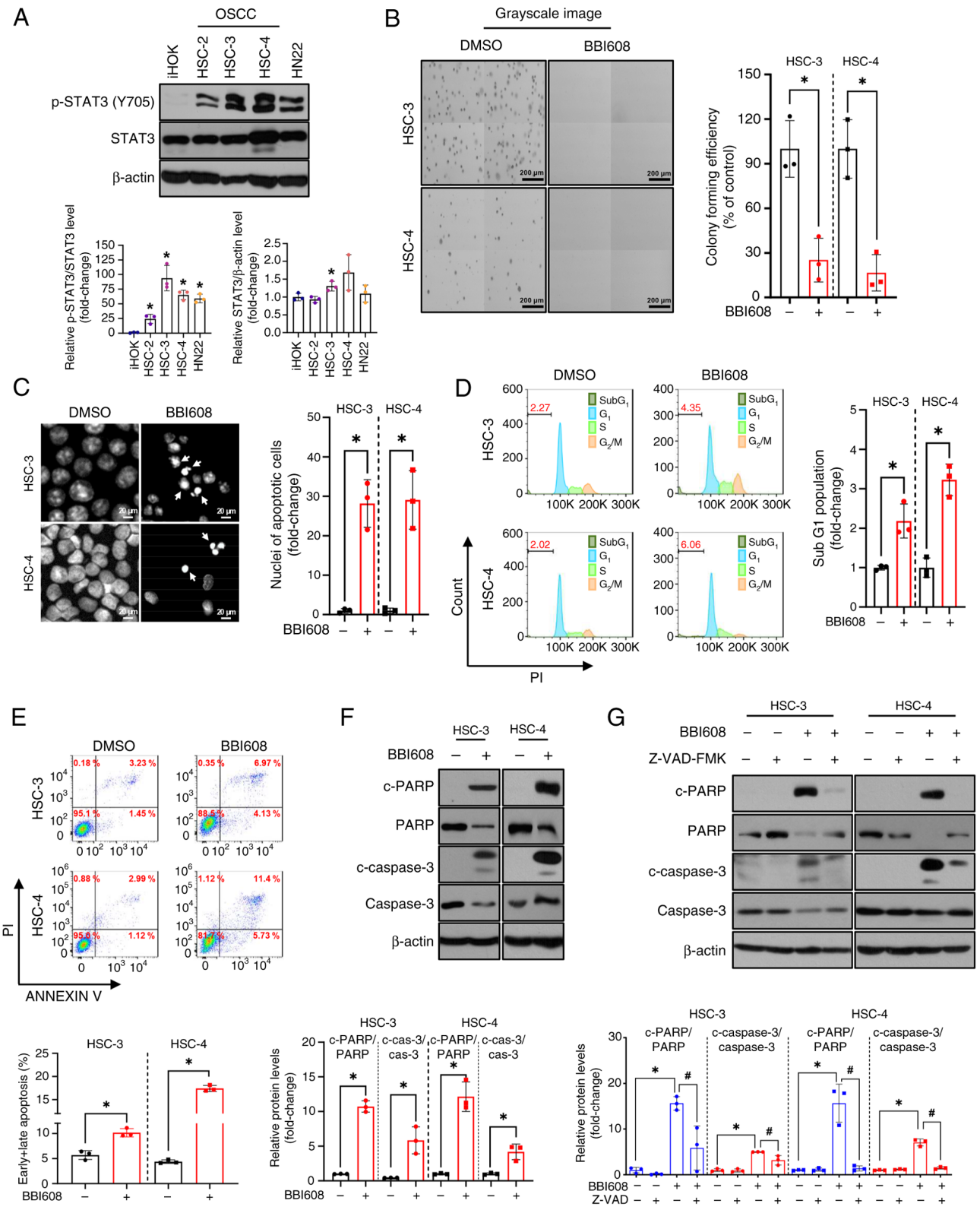

Figure 1. Growth inhibitory activity and apoptotic effects of BBI608 in OSCC cell lines. (A) Protein levels of p-STAT3 in OSCC cell lines were analyzed by western blotting. The expression levels of total STAT3 were normalized to those of β-actin, while p-STAT3(Y705) levels were normalized to those of total STAT3. (B) HSC-3 and HSC-4 cells were treated with BBI608 at 0.4 and 3.2 μM, respectively, for ~2 weeks. Colony formation assays were performed to assess non-adherent, anchorage-independent growth. (C) HSC-3 and HSC-4 cells were treated with BBI608 at 0.4 and 3.2 μM for 24 h, respectively. Representative images of DAPI staining are shown, with condensed nuclei indicated by white arrows. (D) Cell cycle evaluation of OSCC cell lines was performed using flow cytometry analysis with PI staining. The horizontal axis represents PI staining intensity, and the vertical axis represents cell counts. (E) Apoptotic cell death was evaluated by Annexin V/PI staining. The horizontal axis shows Annexin V intensity, and the vertical axis shows PI intensity. (F) HSC-3 and HSC-4 cells were treated with BBI608 at 0.6 and 3.2 μM for 24 h, respectively. The expression levels of c-PARP and c-caspase 3, total PARP, total caspase 3 and β-actin (loading control) were analyzed. The expression levels of c-PARP and c-caspase 3 levels were normalized to those of total PARP and caspase 3, respectively. (G) HSC-3 and HSC-4 cells were pre-treated with Z-VAD-FMK at 10 and 5 μM for 1 h, followed by treatment with BBI608 at 0.6 and 3.2 μM for 24 h, respectively. All experiments were conducted in triplicate and the results are presented as the mean ± SD. *P<0.05 vs. iHOK cells (panel A) or as indicated (panels B-G); #P<0.05. OSCC, oral squamous cell carcinoma; p, phosphorylated; c, cleaved; PARP, poly(ADP-ribose) polymerase; cas, caspase.

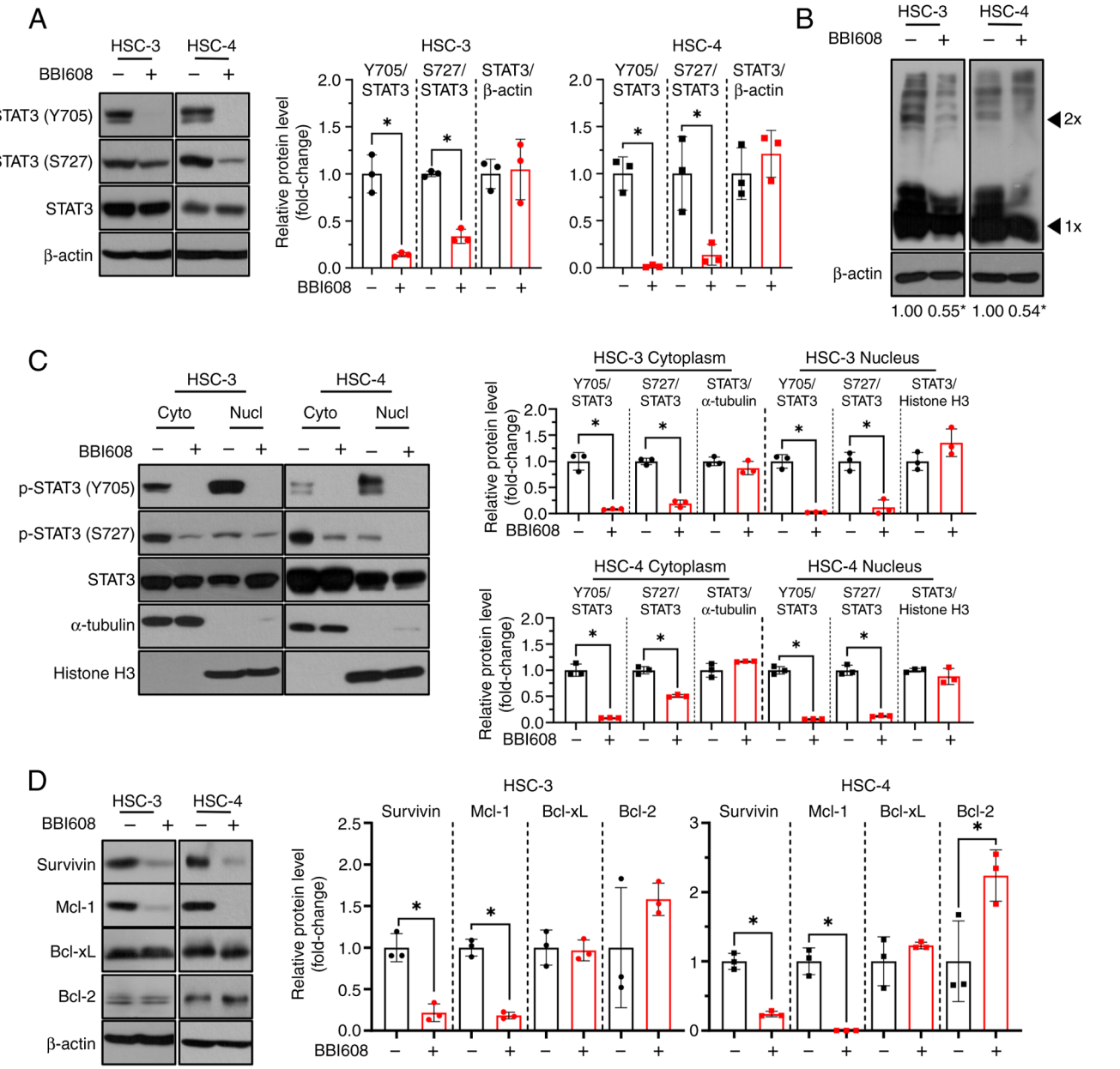

Figure 2. Inhibitory effect of BBI608 on STAT3 signaling in oral squamous cell carcinoma cell lines. (A) Western blot analysis showing the expression levels of p-STAT3, STAT3 and β-actin. The expression levels of total STAT3 were normalized to those of β-actin, while p-STAT3 levels were normalized to those of total STAT3. (B) STAT3 dimerization was assessed by western blot analysis following treatment with bismaleimidohexane (a cross-linker) and normalized to β-actin. (C) Cytoplasmic and nuclear fractionation was performed to examine the levels p-STAT3 in the nucleus after BBI608 treatment. α-tubulin and histone H3 were used as loading controls for the cytoplasmic and nuclear fractions, respectively. The expression levels of total STAT3 were normalized to those of α-tubulin and histone H3, while p-STAT3 levels were normalized to those of total STAT3. (D) Western blot analysis showing the expression of STAT3-regulated anti-apoptotic proteins and β-actin (loading control). All experiments were performed in triplicate, and the results are presented as the mean ± SD. *P<0.05 vs. the (-) group or as indicated. Mcl-1, myeloid cell leukemia-1; p, phosphorylated.

BBI608 modulates the expression of Mcl-1 at the post-translational level. The stability of the Mcl-1 protein can be influenced by proteasomal degradation (27). Although BBI608 increased Mcl-1 mRNA levels, it was further investigated whether Mcl-1 expression is regulated post-translationally by BBI608 treatment. To examine this, HSC-3 and HSC-4 cells were co-treated with the protein synthesis inhibitor CHX at time points (6 h for HSC-3 and 3 h for HSC-4) when Mcl-1 protein levels begin to decline following BBI608 treatment (Fig. S6). The results showed that Mcl-1 protein levels decreased more rapidly with CHX plus BBI608 treatment compared with those observed with CHX plus DMSO treatment (Fig. 4A). To further confirm whether BBI608 affects Mcl-1 protein levels at the post-translational level, cells were co-treated with the proteasomal inhibitor MG132. The results indicated that combining MG132 with BBI608 partially reversed the reduction in Mcl-1 expression caused by BBI608 alone (Fig. 4B). To elucidate how BBI608 induces Mcl-1 protein degradation, the levels of p-Mcl-1, p-GSK3β and p-ERK were evaluated. However, BBI608 decreased the level of p-Mcl-1, increased the level of p-GSK3β, and did not alter the level of p-ERK (Fig. S7). These findings suggested that BBI608 may regulate

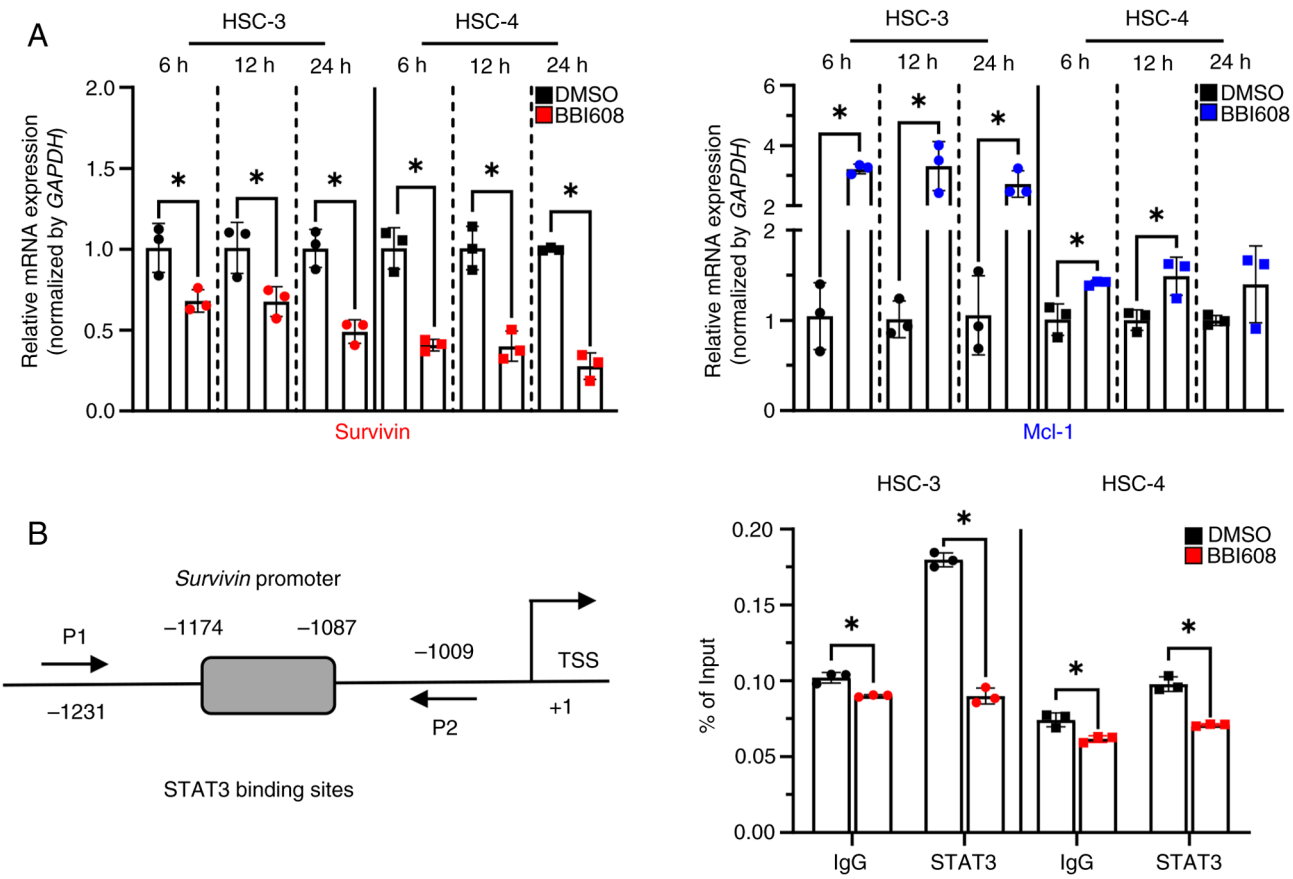

Figure 3. Effect of BBI608 on survivin expression in oral squamous cell carcinoma cell lines. To investigate changes in mRNA levels of survivin and Mcl-1 in response to BBI608, HSC-3, and HSC-4 cells were treated with BBI608 at concentrations of 0.6 and 3.2 μM for 6 to 24 h. (A) RT-qPCR analysis showed a decrease in survivin mRNA levels and an increase in Mcl-1 mRNA levels following BBI608 treatment. The data were normalized to the expression of the housekeeping gene GAPDH. (B) Schematic diagram of STAT3-binding sites and ChIP primer locations on the survivin promoter. HSC-3 and HSC-4 cells were treated with BBI608 at 0.6 and 3.2 μM, respectively, for 24 h. To confirm the presence of STAT3 at the survivin promoter region, a ChIP assay coupled with RT-qPCR on the survivin promoter region was performed. Data are presented as % of input. All experiments were performed in triplicate, and the results are presented as the mean ± SD. *P<0.05. TSS, transcription start site; RT-qPCR, reverse transcription-quantitative PCR; Mcl-1, myeloid cell leukemia-1; ChIP, chromatin immunoprecipitation; P1, survivin ChIP sense; P2, survivin ChIP antisense.

Mcl-1 expression through a post-translational mechanism in OSCC cell lines.

BBI608 effectively triggers apoptosis and impairs STAT3 signaling in OSCC spheroids. Since spheroid cultures closely mimic the hypoxic and proliferative characteristics of *in vivo* tumors, they serve as a valuable model for screening potential drug candidates (15,28). Therefore, it was investigated whether BBI608 exhibits anticancer effects in 3D cultures of OSCC cell lines. To achieve this, a hanging drop assay was used to establish 3D cultures of OSCC cell lines. Consistent with the results from 2D cultures, BBI608 demonstrated robust growth inhibitory activity in both OSCC spheroids (Fig. 5A), which was further confirmed by live/dead assay showing that BBI608 increased the number of dead cells (red color) in both cell lines (Fig. 5B). Additionally, BBI608 effectively induced apoptosis in OSCC spheroids, as evidenced by the increased cleavage of PARP and caspase 3, as well as the higher number of apoptotic cells following BBI608 treatment (Fig. 5C and D). Subsequently, western blotting and RT-qPCR were performed to determine whether and/or how BBI608 inhibits STAT3 signaling in OSCC spheroids. The results showed that BBI608 had an inhibitory effect on STAT3 signaling in OSCC 3D spheroids (Fig. 5E). Interestingly, BBI608 reduced survivin mRNA levels in both OSCC spheroids and significantly decreased Mcl-1 mRNA levels only in HSC-4 spheroids (Fig. 5F). Overall, these results indicated that BBI608 induced apoptosis and significantly inhibited STAT3 signaling in OSCC spheroids.

Discussion

Aberrant upregulation of STAT3, which is commonly observed in various cancers, including hepatocellular carcinoma and non-Hodgkin's lymphoma, is associated with numerous malignant activities, including tumorigenesis and enhanced cell survival (24,29). This is consistent with our previous study showing that p-STAT3 levels are significantly upregulated in tissues from patients with OSCC compared with normal oral mucosa (9). Mounting evidence indicates that STAT3 is essential for early embryonic development, whereas conditional deletion of the STAT3 gene in adult mouse tissues results in only minor phenotypes, including defects during the second hair cycle and thymic hypoplasia (5,30). This suggests that STAT3 represents an attractive therapeutic target for cancer therapy. In the present study, BBI608 exerted a marked

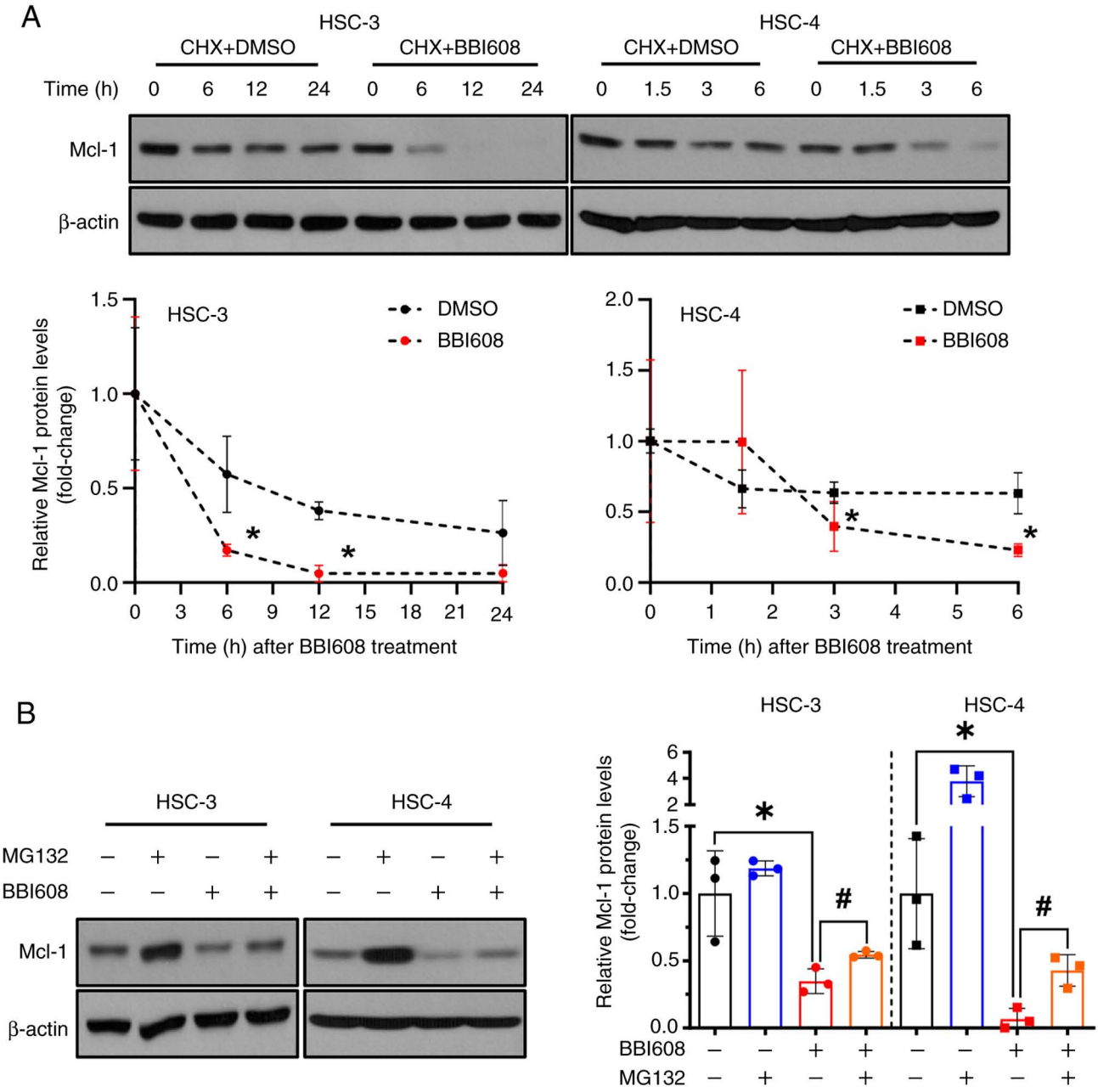

Figure 4. Effect of BBI608 on Mcl-1 expression in oral squamous cell carcinoma cell lines. (A) HSC-3 and HSC-4 cells were pretreated with CHX at concentrations of 50 and 100 ng/ml for 1 h, respectively. Following this, the cells were treated with BBI608 at concentrations of 0.6 and 3.2 μM for the designated periods of time, respectively. (B) HSC-3 and HSC-4 cells were pretreated with MG-132 at concentrations of 300 and 500 nM for 1 h, respectively, and then treated with BBI608 at 0.6 and 3.2 μM for 24 h. The data were normalized to the expression of β-actin. All experiments were performed in triplicate, and the results are presented as mean ± SD. *P<0.05 vs. DMSO or as indicated; #P<0.05. CHX, cycloheximide; Mcl-1, myeloid cell leukemia-1.

inhibitory effect on STAT3 activity in OSCC cell lines, leading to pronounced apoptotic cell death. Given the potent anticancer effects of BBI608 observed in multiple studies and its approval for the treatment of advanced gastric and gastroesophageal junction adenocarcinoma (10,11,31), the present results raise the possibility that BBI608 may be applied to clinical trials in patients with OSCC.

The proteasomal degradation of Mcl-1, which involves its phosphorylation and subsequent ubiquitination, is regulated by several signaling pathways, including ERK and GSK3β (27). Especially, GSK3β-mediated hyper-phosphorylation of Mcl-1 at Ser159, together with Thr163 phosphorylation, promotes its proteasomal degradation (32). However, the present results showed that BBI608 decreased the level of p-Mcl-1, indicating that the post-translational modulation of Mcl-1 by BBI608 was not associated with its phosphorylation. To rule out the involvement of GSK3β and ERK pathways in Mcl-1 degradation, the levels of these kinases were also examined, but the result was not consistent with this hypothesis. Previous research demonstrated that the activation of MAPK by reactive oxygen species (ROS) influences Mcl-1 stability in response to BBI608 and increases Noxa protein expression in a concentration-dependent manner (33). Since Noxa can bind to the hydrophobic groove of Mcl-1 through its BH3 domain, making Mcl-1 accessible to ubiquitin ligases and leading to its ubiquitination and proteasomal degradation (32), it is possible that BBI608 modulates

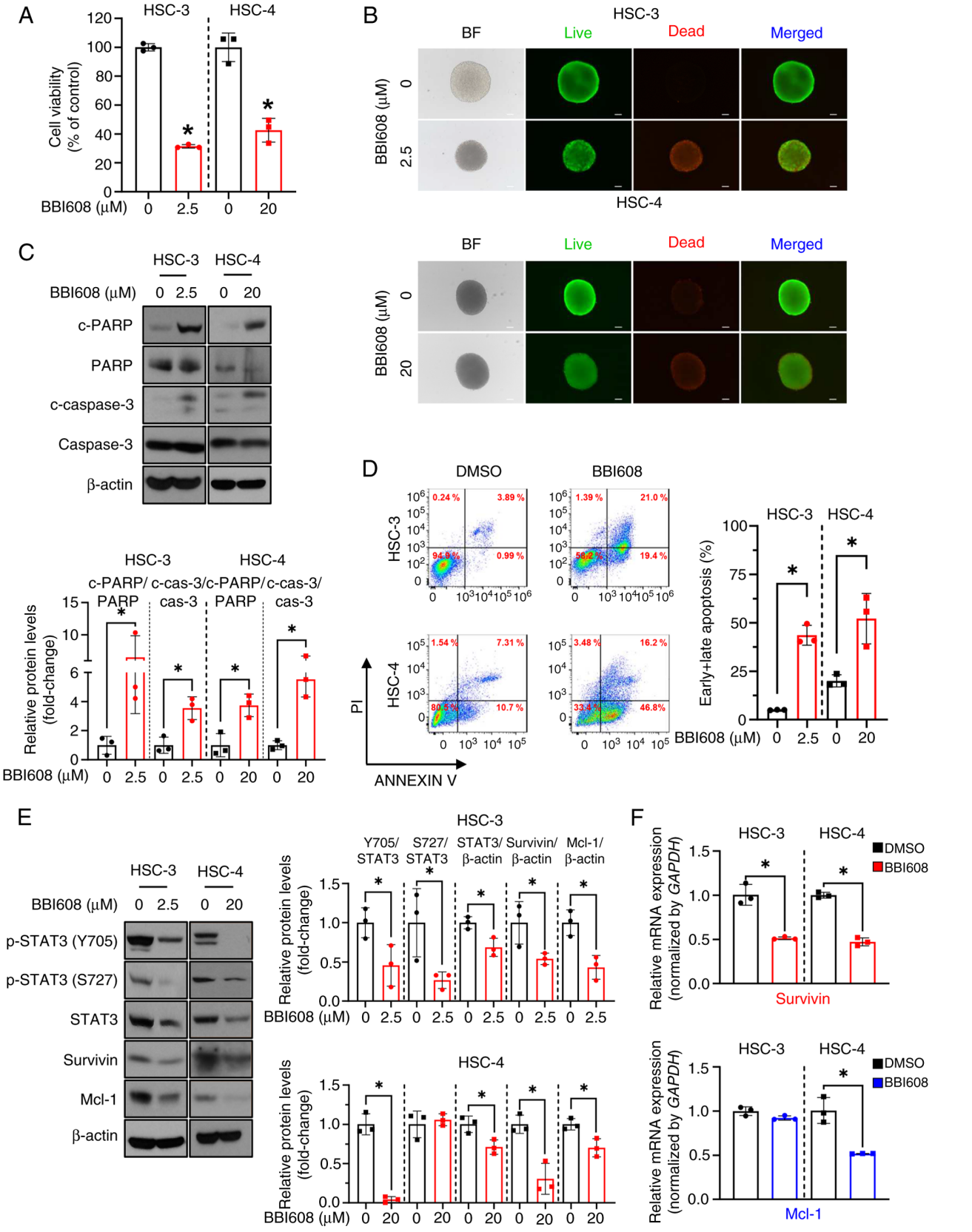

Figure 5. Inhibitory effects of BBI608 on the growth of OSCC spheroids and STAT3 signaling. HSC-3 and HSC-4 cells were treated with BBI608 at concentrations of 2.5 and 20 μM for 24 h, respectively. Cell viability of OSCC spheroids was assessed to determine the cytotoxic effects of BBI608 using (A) Cell Counting Kit-8 and (B) live/dead assays (magnification, x100; scale bar, 100 μm). Apoptotic cell death in OSCC spheroids was evaluated by (C) the expression of c-PARP and c-caspase 3 and (D) Annexin V/PI staining. The horizontal axis represents Annexin V staining, while the vertical axis represents PI staining. (E) Western blot analysis indicated the expression levels of STAT3-regulated proteins along with β-actin. Protein expression levels were normalized to β-actin, except for p-STAT3 levels, which were normalized to those of total STAT3. (F) The mRNA levels of survivin and Mcl-1 in OSCC spheroids were analyzed using reverse-transcription-quantitative PCR. The data were normalized to the expression of the housekeeping gene GAPDH. All experiments were performed in triplicate, and the results are presented as the mean ± SD. *P<0.05. OSCC, oral squamous cell carcinoma; Mcl-1, myeloid cell leukemia-1; p, phosphorylated; c, cleaved; PARP, poly(ADP-ribose) polymerase; cas, caspase; BF, bright field.

Mcl-1 protein stability, at least in part, through Noxa-mediated ubiquitination in OSCC cell lines. However, this needs to be examined in future studies. Interestingly, it was observed that Mcl-1 mRNA expression increased following BBI608 treatment. Considering that Mcl-1 stability was significantly decreased by proteasomal degradation, it may be hypothesized that complementary feedback mechanisms, intrinsic to cellular homeostasis, take place against the downregulation of Mcl-1 protein by BBI608 treatment.

The present study revealed that total STAT3 expression remained unchanged in 2D culture, while a significant reduction was observed in 3D culture following BBI608 treatment. Similarly, Mcl-1 mRNA expression decreased in HSC-4 spheroids but not in 2D culture. These findings contrast those of a previous study, which reported that BBI608 eliminated total STAT3 expression in glioma stem cells in both 2D and 3D culture systems (34). The differences between 2D and 3D cultures, including variations in cell polarity, as well as cell-cell and cell-extracellular environment interactions, result in changes in gene expression and signaling pathways (35). It must also be noted that 3D spheroids exhibit lower proliferation rates and more hypoxic conditions compared with 2D cultures (36). These factors may lead to discrepancies in drug responses, as altered cellular properties can affect the efficacy of treatments that rely on active cell division or oxygen availability. For example, a previous study observed that the anti-proliferative effect of 5-fluorouracil was more pronounced in 2D culture than in 3D culture, whereas the hypoxia-activated agent tirapazamine was more effective in 3D culture (37). Consistent with this notion, the present results showed that a higher concentration of BBI608 was required to achieve cytotoxic effects of BBI608 on OSCC 3D spheroids compared with that required for the 2D culture. Furthermore, it has been reported that BBI608 can affect STAT3 expression in osteosarcoma cells by regulating protein synthesis in 2D culture (38). However, given the notion that BBI608 is a potent ROS inducer (11), the possibility that STAT3 stability could be regulated by ROS-mediated proteasomal degradation cannot be ruled out (39). Therefore, further investigation is necessary to determine if the mechanism by which BBI608 exerts differential regulation of STAT3 protein in 2D and 3D culture is context dependent.

In a retrospective study, patients with advanced colorectal cancer treated with BBI608 in cases of elevated p-STAT3 levels in tumor cells and in the tumor microenvironment (TME) exhibited notably prolonged overall survival in comparison with the placebo group (40). Furthermore, BBI608 sensitivity in tumor cells has been demonstrated to result in an increase in STAT3 activity in both the tumor cells and TME (41), suggesting that BBI608 may be more efficient in OSCC cells with high p-STAT3 levels. However, in the present study, BBI608 reduced cell viability in OSCC cells irrespectively of p-STAT3 levels, implying that BBI608-mediated apoptotic cell death may involve other pathways as well as STAT3. According to certain studies, BBI608 may also exhibit off-target effects on other molecules, including AKT/mTOR or MAPK pathways (33,42). Notably, it has been reported that BBI608 could be a substrate for NAD(P)H dehydrogenase [quinone] 1, thereby resulting in ROS-mediated STAT3 inhibition (11), which suggests that these pathways could also contribute to BBI608-mediated antitumor effects, particularly in OSCC cell line with low p-STAT3 levels, where the mechanism of BBI608 is unclear. It is possible that BBI608 may directly bind to STAT3 (although this has not been demonstrated in the literature to the best of our knowledge) or modulate STAT3 indirectly by altering cellular stress responses. Therefore, additional studies are needed to further clarify these off-target effects of BBI608.

The present study demonstrated that BBI608 significantly inhibited STAT3 activation in OSCC cell lines regardless of the culture conditions. Given the important role of STAT3 in OSCC progression and the absence of effective therapeutic options for STAT3 inhibition (7,9), the present findings suggest the potential repurposing of BBI608 for treating patients with OSCC exhibiting high STAT3 activity. However, a limitation of the current study is the absence of preclinical validation in animal models; therefore, future research integrating animal studies may help to further elucidate the therapeutic potential of BBI608 in OSCC. In conclusion, the present study validated the feasibility and efficacy of repurposing BBI608 in 2D and 3D OSCC models. BBI608 demonstrated a potent anticancer effect by inhibiting STAT3 activation and its downstream target genes, survivin and Mcl-1, leading to the induction of apoptosis.

Acknowledgements

Not applicable.

Funding

The present study was supported by the National Research Foundation of Korea grant funded by the Korean government (grant nos. 2022R1A2C1091608 and 2023-00247502).

Availability of data and materials

The data generated in the present study may be requested from the corresponding author.

Authors' contributions

DGP conceived and designed the study, acquired and analyzed the data, and drafted the manuscript. HJK, SL, HMJ and SDH analyzed and interpreted the data. SJC and SDC conceived and designed the study, and reviewed and edited the manuscript. DGP and SDC confirmed the authenticity of all the raw data. All authors read and approved the final manuscript.

Ethics approval and consent to participate

Not applicable.

Patient consent for publication

Not applicable.

Competing interests

The authors declare that they have no competing interests.

References

1. Pushpakom S, Iorio F, Eyers PA, Escott KJ, Hopper S, Wells A, Doig A, Guilliams T, Latimer J, McNamee C, *et al*: Drug repurposing: Progress, challenges and recommendations. Nat Rev Drug Discov 18: 41-58, 2019.
2. Abdelsayed M, Kort EJ, Jovinge S and Mercola M: Repurposing drugs to treat cardiovascular disease in the era of precision medicine. Nat Rev Cardiol 19: 751-764, 2022.
3. Xia Y, Sun M, Huang H and Jin WL: Drug repurposing for cancer therapy. Signal Transduct Tar 9: 92, 2024.
4. Hanahan D: Hallmarks of Cancer: New dimensions. Cancer Discov 12: 31-46, 2022.
5. Hu YM, Dong ZG and Liu KD: Unraveling the complexity of STAT3 in cancer: Molecular understanding and drug discovery. J Exp Clin Canc Res 43: 23, 2024.
6. Yu H and Jove R: The stats of cancer - New molecular targets come of age. Nat Rev Cancer 4: 97-105, 2004.
7. Macha MA, Matta A, Kaur J, Chauhan SS, Thakar A, Shukla NK, Gupta SD and Ralhan R: Prognostic significance of nuclear pSTAT3 in oral cancer. Head Neck-J Sci Spec 33: 482-489, 2011.
8. Wei LY, Lin HC, Tsai FC, Ko JY, Kok SH, Cheng SJ, Lee JJ and Chia JS: Effects of interleukin-6 on STAT3-regulated signaling in oral cancer and as a prognosticator of patient survival. Oral Oncol 124: 105665, 2022.
9. Kim LH, Khadka S, Shin JA, Jung JY, Ryu MH, Yu HJ, Lee HN, Jang B, Yang IH, Won DH, *et al*: Nitidine chloride acts as an apoptosis inducer in human oral cancer cells and a nude mouse xenograft model via inhibition of STAT3. Oncotarget 8: 91306-91315, 2017.
10. Li Y, Rogoff HA, Keates S, Gao Y, Murikipudi S, Mikule K, Leggett D, Li W, Pardee AB and Li CJ: Suppression of cancer relapse and metastasis by inhibiting cancer stemness. Proc Natl Acad Sci USA 112: 1839-1844, 2015.
11. Froeling FEM, Swamynathan MM, Deschenes A, Chio IIC, Brosnan E, Yao MA, Alagesan P, Lucito M, Li J, Chang AY, *et al*: Bioactivation of napabucasin triggers reactive oxygen species-mediated cancer cell death. Clin Cancer Res 25: 7162-7174, 2019.
12. Bendell JC, Hubbard JM, O'Neil BH, Jonker DJ, Starodub A, Peyton JD, Pitot HC, Halfdanarson TR, Nadeau BR, Zubkus JD, *et al*: Phase 1b/II study of cancer stemness inhibitor napabucasin (BBI-608) in combination with FOLFIRI+/-bevacizumab (bev) in metastatic colorectal cancer (mCRC) patients (pts). J Clin Oncol, 2017.
13. Bekaii-Saab TS, Starodub A, El-Rayes BF, Shahda S, O'Neil BH, Noonan AM, Shaib WL, Hanna WT, Mikhail S, Neki AS, *et al*: Phase 1b/2 trial of cancer stemness inhibitor napabucasin (NAPA)+ nab-paclitaxel (nPTX) and gemcitabine (Gem) in metastatic pancreatic adenocarcinoma (mPDAC). J Clin Oncol 36 (Suppl 15): 4110, 2018.
14. Shao Z, Wang H, Ren H, Sun Y and Chen X: The anticancer effect of napabucasin (BBI608), a natural naphthoquinone. Molecules 28: 5678, 2023.
15. Ware MJ, Colbert K, Keshishian V, Ho J, Corr SJ, Curley SA and Godin B: Generation of homogenous three-dimensional pancreatic cancer cell spheroids using an improved hanging drop technique. Tissue Eng Part C-Me 22: 312-321, 2016.
16. Oner E, Gray SG and Finn SP: Cell viability assay with 3d prostate tumor spheroids. Methods Mol Biol 2645: 263-275, 2023.
17. Yu HJ, Park C, Kim SJ, Cho NP and Cho SD: Signal transducer and activators of transcription 3 regulates cryptotanshinone-induced apoptosis in human mucoepidermoid carcinoma cells. Pharmacogn Mag 10: 622-629, 2014.
18. Livak KJ and Schmittgen TD: Analysis of relative gene expression data using real-time quantitative PCR and the 2(-Delta Delta C(T)) method. Methods 25: 402-408, 2001.
19. Gritsko T, Williams A, Turkson J, Kaneko S, Bowman T, Huang M, Nam S, Eweis I, Diaz N, Sullivan D, *et al*: Persistent activation of STAT3 signaling induces survivin gene expression and confers resistance to apoptosis in human breast cancer cells. Clin Cancer Res 12: 11-19, 2006.
20. Riccardi C and Nicoletti I: Analysis of apoptosis by propidium iodide staining and flow cytometry. Nat Protoc 1: 1458-1461, 2006.
21. Kim HJ, Shin JA, Lee YG, Jin B, Lee WW, Lee Y, Choi SJ, Han JM, Ahn MH, Kim JH, *et al*: Zingiber officinale promotes autophagy and apoptosis in human oral cancer through the C/EBP homologous protein. Cancer Sci 115: 2701-2717, 2024.
22. Won DH, Kim LH, Jang B, Yang IH, Kwon HJ, Jin B, Oh SH, Kang JH, Hong SD, Shin JA and Cho SD: In vitro and in vivo anti-cancer activity of silymarin on oral cancer. Tumour Biol 40: 1010428318776170, 2018.
23. Yang IH, Hong SH, Jung M, Ahn CH, Yoon HJ, Hong SD, Cho SD and Shin JA: Cryptotanshinone chemosensitivity potentiation by TW-37 in human oral cancer cell lines by targeting STAT3-Mcl-1 signaling. Cancer Cell Int 20: 405, 2020.
24. Johnson DE, O'Keefe RA and Grandis JR: Targeting the IL-6/JAK/STAT3 signalling axis in cancer. Nat Rev Clin Oncol 15: 234-248, 2018.
25. Hsieh FC, Cheng G and Lin J: Evaluation of potential Stat3-regulated genes in human breast cancer. Biochem Bioph Res Co 335: 292-299, 2005.
26. Zou SL, Tong QY, Liu BW, Huang W, Tian Y and Fu XH: Targeting STAT3 in cancer immunotherapy. Mol Cancer 19: 145, 2020.
27. Wang H, Guo M, Wei H and Chen Y: Targeting MCL-1 in cancer: Current status and perspectives. J Hematol Oncol 14: 67, 2021.
28. Breslin S and O'Driscoll L: Three-dimensional cell culture: The missing link in drug discovery. Drug Discov Today 18: 240-249, 2013.
29. Geiger JL, Grandis JR and Bauman JE: The STAT3 pathway as a therapeutic target in head and neck cancer: Barriers and innovations. Oral Oncol 56: 84-92, 2016.
30. Levy DE and Lee CK: What does Stat3 do? J Clin Invest 109: 1143-1148, 2002.
31. Becerra C, Stephenson J, Jonker DJ, Cohn AL, Asmis TR, Bekaii-Saab TS, Conkling PR, Garbo LE, Lenz HJ, *et al*: Phase Ib/II study of cancer stem cell (CSC) inhibitor BBI608 combined with paclitaxel in advanced gastric and gastroesophageal junction (GEJ) adenocarcinoma. J Clin Oncol 33 (Suppl 15): 4069, 2015.
32. Senichkin VV, Streletskaia AY, Gorbunova AS, Zhivotovsky B and Kopeina GS: Saga of Mcl-1: Regulation from transcription to degradation. Cell Death Differ 27: 405-419, 2020.
33. Li X, Wei YQ and Wei XW: Napabucasin, a novel inhibitor of STAT3, inhibits growth and synergises with doxorubicin in diffuse large B-cell lymphoma. Cancer Lett 491: 146-161, 2020.
34. Han D, Yu T, Dong N, Wang B, Sun F and Jiang D: Napabucasin, a novel STAT3 inhibitor suppresses proliferation, invasion and stemness of glioblastoma cells. J Exp Clin Cancer Res 38: 289, 2019.
35. Zajączkowska M, Teresiak A, Filas V, Ibbs M, Bliźniak R, Łuczewski Ł and Lamperska K: 2D and 3D cell cultures - A comparison of different types of cancer cell cultures. Arch Med Sci 14: 910-919, 2018.
36. Edmondson R, Broglie JJ, Adcock AF and Yang LJ: Three-dimensional cell culture systems and their applications in drug discovery and cell-based biosensors. Assay Drug Dev Techn 12: 207-218, 2014.
37. Tung YC, Hsiao AY, Allen SG, Torisawa YS, Ho M and Takayama S: High-throughput 3D spheroid culture and drug testing using a 384 hanging drop array. Analyst 136: 473-478, 2011.
38. Zuo D, Shogren KL, Zang J, Jewison DE, Waletzki BE, Miller AL II, Okuno SH, Cai Z and Yaszemski MJ: Inhibition of STAT3 blocks protein synthesis and tumor metastasis in osteosarcoma cells. J Exp Clin Cancer Res 37: 244, 2018.
39. Kim J, Park A, Hwang J, Zhao X, Kwak J, Kim HW, Ku M, Yang J, Kim TI, Jeong KS, *et al*: KS10076, a chelator for redox-active metal ions, induces ROS-mediated STAT3 degradation in autophagic cell death and eliminates ALDH1 stem cells. Cell Rep 40: 111077, 2022.
40. Jonker DJ, Nott L, Yoshino T, Gill S, Shapiro J, Ohtsu A, Zalcberg J, Vickers MM, Wei AC, Gao Y, *et al*: Napabucasin versus placebo in refractory advanced colorectal cancer: A randomised phase 3 trial. Lancet Gastroenterol 3: 263-270, 2018.
41. Chang AY, Hsu E, Patel J, Li Y, Zhang M, Iguchi H and Rogoff HA.: Evaluation of tumor cell-tumor microenvironment component interactions as potential predictors of patient response to napabucasin. Mol Cancer Res 17: 1429-1434, 2019.
42. Petsri K, Thongsom S, Racha S, Chamni S, Jindapol S, Kaekratoke N, Zou H and Chanvorachote P: Novel mechanism of napabucasin, a naturally derived furanonaphthoquinone: Apoptosis and autophagy induction in lung cancer cells through direct targeting on Akt/mTOR proteins. Bmc Complement Med 22: 250, 2022.